THE JOURNAL OF PHYSICAL CHEMISTRY C

Article

pubs.acs.org/JPCC

Differentiating Intrinsic Reactivity of Copper, Copper−Zinc Alloy, and Copper/Zinc Oxide Interface for Methanol Steam Reforming by First-Principles Theory

Sha-Sha Wang,[†,∥,⊥] Hai-Yan Su,[†,⊥] Xiang-Kui Gu,[†] and Wei-Xue Li*[,†,‡,§]

[†]State Key Laboratory of Catalysis, State Key Laboratory of Molecular Reaction Dynamics, Dalian Institute of Chemical Physics, Chinese Academy of Sciences, Dalian 110623, China

[‡]Department of Chemical Physics, iChEM, University of Science and Technology of China, Hefei 230026, China

[§]CAS Excellence Center for Nanoscience, Hefei National Laboratory for Physical Sciences at Microscale, Hefei 230026, China

[∥]University of Chinese Academy of Sciences, Shijingshan District, Beijing 100049, China

Supporting Information

ABSTRACT: Identifying the intrinsic activity of the distinct sites which coexist in oxide-supported metal particles is vital but challenging for rational design of catalysts. We treat the challenge here by density functional theory calculations to differentiate unbiasedly the intrinsic reactivity of a variety of sites observed under reaction conditions for methanol steam reforming on Cu/ZnO catalyst. Metallic Cu and CuZn alloy are found to be less active but highly selective toward formaldehyde because water dissociation is demanding, which limits the formation of hydroxyl and subsequent coupling necessary to yield CO_2. Cu/ZnO interface is highly active and selective for H_2/CO_2 because of its superior activity for water and methanol activation. Distinct hydrogen affinity at Cu/ZnO interface also leads to more favorable CO_2 production via H_2COO, in contrast to via HCOOH at (bi)metallic sites. The distinct reactivity of various structural motifs exposed and the importance of the metal/oxide for selectivity revealed is valuable for optimal design of catalysts.

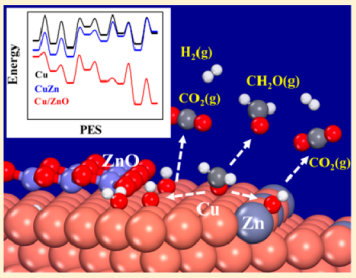

1. INTRODUCTION

Methanol steam reforming (MSR) provides a promising scheme for generation of hydrogen in various important processes, such as fuel cells and hydrogenolysis of biomass-based compounds.[1−3] In this reaction, the high H_2 and CO_2 selectivities are critical to avoid the poisoning of the fuel-cell Pt anode by CO byproduct and to maximize the hydrogen yield.[4−6] The Cu/ZnO catalyst originally designed for methanol synthesis exhibits high activity and selectivity toward H_2 and CO_2 for MSR. However, the coexistence of a variety of structural motifs/sites, such as Cu, ZnO, CuZn alloy, and Cu/ZnO interface, results in the identification of active sites to be elusive.[7−12] For methanol synthesis on Cu/ZnO, there are similar structural motifs coexisting under reaction conditions, and it remains a hot topic of debate, along with which sites are the active sites.[13−18]This severely prevents the mechanistic understanding and rational design of catalysts. So far, preparing the supported metal particles with identical sites still represents a significant challenge in catalyst synthesis. The site homogeneity might be worsened further by considering strong-metal-support interaction, which leads to the formation of various uncontrolled boundaries and dynamic response of the supported catalysts under reaction conditions, such as (de)alloying, reactant-induced segregation, oxidation, and reduction just to name a few. We treat the challenge here by density functional theory (DFT) calculations to differentiate unbiasedly the intrinsic reactivity of the various structural motifs/sites observed under reaction conditions.

In MSR, the main detected products include CO, CH_2O, CO_2, and H_2.[19] Among these, CH_2O and CO come from the partial and complete dehydrogenation of CH_3OH.[20−23] In the case of CO_2/H_2 formation, it is generally suggested to be through the reaction of H_2O with CO from methanol decomposition, and the CO_2 selectivity is determined by the reaction balance of water gas shift reaction.[7,8,24] Alternatively, a more favorable pathway has been reported recently,[25−28] where CH_2O* produced by methanol partial dehydrogenation can recombine with OH* or O* from water dissociation, leading to the formation of hydroxyl methoxy (H_2COOH*) or dioxomethylene (H_2COO*) intermediate. The intermediates then dehydrogenate sequentially to CO_2, and for H_2COOH* dehydrogenation discrepancy exists between an initial O−H bond scission (via H_2COO*) and C−H bond scission (via HCOOH*).

To differentiate the intrinsic MSR reactivity on the various sites of Cu/ZnO catalyst observed under reaction conditions, we present an unbiased DFT study of MSR pathway on Cu(111), CuZn alloy, and Cu/ZnO interface (see Computational Methods section for a more detailed description of the

Received: August 3, 2017
Revised: September 12, 2017
Published: September 19, 2017

DOI: 10.1021/acs.jpcc.7b07703
J. Phys. Chem. C 2017, 121, 21553−21559

models). Since CuZn alloy has been shown to be formed preferentially on stepped Cu,[16,29] we use the Cu(211) surface with Zn substitution of 33% Cu at the step edge to simulate CuZn alloy (Figure 1a). For Cu/ZnO interface, the planar, graphite-like ZnO layer supported on Cu(111) (Figure 1b) is adopted, where the similar structures have been identified on Au(111) and Cu nanoparticles in an industrially relevant Cu/ZnO/Al_2O_3 catalyst.[30−33] Despite the high CO_2 selectivity, the pristine ZnO is not considered here owing to its low activity for MSR.[34]

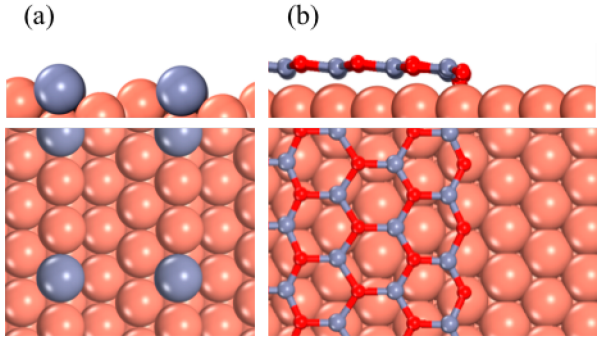

Figure 1. Side view (upper panel) and top view (lower panel) of (a) CuZn(211) and (b) graphite-like ZnO on Cu for Cu/ZnO interface. The vermilion, red, and purple balls represent Cu, O, and Zn atoms, respectively.

2. COMPUTATIONAL METHODS

DFT calculations were performed by the Vienna ab-initio simulation package (VASP)[35] with optPBE-vdW.[36] The interaction between the ionic cores and electrons was described by the projector-augmented wave (PAW) method,[37,38] and the Kohn−Sham valence electronic wave function was expanded in a plane-wave basis set with a kinetic energy cutoff at 400 eV. The energies were converged to within 10^{-4} eV/atom, and the forces were converged to within 0.02 eV/Å.

The Cu(111) surface was modeled using a four-layer slab with (3 × 3) surface unit cell. A (1 × 3)-11-layer Cu(211) slab with 1/3 Cu substituted by Zn on the step edge, denoted as CuZn(211), was used to simulate CuZn alloy.[15,39] One-layer graphite-like (3 × 3) ZnO(0001) ribbon, with an in-plane lattice of 3.30 Å, on three-layer (4 × 8) Cu(111) slab was adopted to simulate Cu/ZnO interface according to previous results.[30,32,33,40,41] A vacuum region of 15 Å between any two repeated slabs was found to be sufficient to avoid interactions between repeated slabs along the z-direction. The surface Brillouin zone was sampled with a (5 × 5 × 1), (5 × 5 × 1), and (1 × 2 × 1) Monkhorst−Pack k-points grid mesh[42] for Cu(111), CuZn(211), and Cu/ZnO, respectively. The top two layers of Cu(111) and Cu/ZnO, top six layers of CuZn(211), and the adsorbed species were fully relaxed, and the remaining layers were fixed in their bulk truncated positions. The lattice constant for copper is calculated to be 3.64 Å, in good agreement with the experimental value of 3.62 Å.

The adsorption energies (E_{ads}) were calculated at their most stable structures, relative to the clean surfaces and the isolated atoms

$$E_{ads} = E_{ads/sub} - E_{ads} - E_{sub}$$

in which $E_{ad/sub}$, E_{ad}, and E_{sub} are the energy of the optimized adsorption system of adsorbate and substrate, adsorbate in the gas phase, and the clean substrate, respectively.

All transition states (TSs) were located by the force reversed method[43] and climbing-image nudged elastic band method (CI-NEB).[44,45] We also performed DFT+U calculations for the correction of the on-site Coulomb repulsion of 3d electrons of Zn atoms. We have tested the two commonly used $U - J$ values of 4.7 eV[46] and 8.5 eV[47] for Zn in Au(111)/ZnO and found that both values gave rather similar structures and energetics.[32] Therefore, a value of $U - J$ = 4.7 eV was used in the present work. The relaxation will stop until the residual forces in each atom are smaller than 0.05 eV/Å. The transition states were verified by vibrational analysis showing a single imaginary mode. Zero-point energies and entropy corrections were neglected. The activation energies (E_a) and reaction energies of elementary reactions (E_r) were taken with respect to isolated reactants/products. The negative values of E_r represent exothermic processes, and positive values of E_r represent endothermic processes.

Table 1. Calculated Activation Energies (E_a in eV), Reaction Energies (E_r in eV), and Geometric Information (d in Å) at the Transition States of the Elementary Reactions Involved in MSR on Cu(111), CuZn(211), and Cu(111)/ZnO Interface

	Cu(111)			CuZn(211)			Cu(111)/ZnO		
elementary reactions	E_a	E_r	d	E_a	E_r	d	E_a	E_r	d
(1) $H_2O^* + * \rightarrow OH^* + H^*$	1.18	−0.14	1.42	0.81	−0.21	1.39	0.17	−0.70	1.12
(2) $OH^* + * \rightarrow O^* + H^*$	1.70	0.60	1.57	1.53	0.76	1.67	0.60	−0.21	1.25
(3) $CH_3OH^* + * \rightarrow CH_3O^* + H^*$	1.07	−0.18	1.43	0.74	−0.11	1.41	0.28	−0.52	1.12
(4) $CH_3O^* + * \rightarrow CH_2O^* + H^*$	1.33	0.99	1.83	1.29	1.03	1.93	1.27	0.58	1.54
(5) $OH^* + CH_2O^* \rightarrow H_2COOH^* + *$	0.38	−0.39	2.11	0.20	−0.31	1.96	0.38	−0.53	2.11
(6) $H_2COOH^* + * \rightarrow HCOOH + H^*$	0.92	0.07	1.60	0.91	0.22	1.73	1.33	0.19	1.40
(7) $HCOOH^* + * \rightarrow HCOO^* + H^*$	0.53	−0.51	1.54	0.62	−0.63	1.43	0	−1.27	
(8) $HCOO^* + * \rightarrow CO_2^* + H^*$	1.26	0.51	1.53	1.45	0.86	1.87	1.19	0.04	1.40
(9) $H_2COOH^* + * \rightarrow H_2COO^* + H^*$	1.20	0.21	1.60	1.34	0.12	1.47	0.14	−0.09	1.22
(10) $H_2COO^* + * \rightarrow HCOO^* + H^*$	0.81	−0.64	1.52	1.09	−0.52	1.54	0.91	−0.99	1.34
(11) $CH_2O^* + * \rightarrow HCO^* + H^*$	0.83	0.31	1.63	0.81	0.25	1.63	0.53	−0.30	1.42
(12) $HCO^* + * \rightarrow CO^* + H^*$	0.29	−0.76	1.42	0.45	−0.52	1.46	0.20	−1.34	1.25
(13) $H^* + H^* \rightarrow H_2$ (g) + 2*	0.90	0.36	0.95	0.85	−0.34	1.44			
(14) $O_{ZnO}H^* + * \rightarrow O_{ZnO} + H^*$							1.34	0.53	1.62

DOI: 10.1021/acs.jpcc.7b07703
J. Phys. Chem. C 2017, 121, 21553−21559

3. RESULTS AND DISCUSSION

We first investigate water dissociation on Cu(111), CuZn(211), and Cu/ZnO interface. It can be seen from Table 1 that not only is the $H_2O^* + * \rightarrow OH^* + H^*$ step more exothermic on Cu/ZnO interface compared with that on Cu(111) and CuZn(211), but the activation energy barrier E_a is also decreased by 1.01 and 0.64 eV on Cu/ZnO interface. Figure 2a shows further that Cu/ZnO interface stabilizes the transition

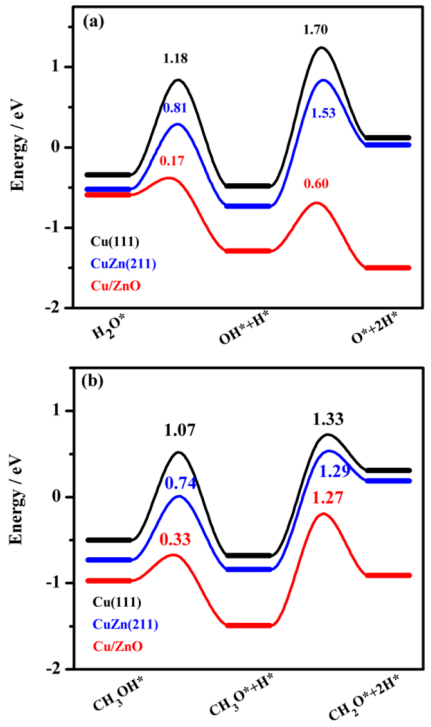

Figure 2. Energy profiles of (a) water dissociation and (b) formaldehyde formation on Cu(111) (black line), CuZn(211) (blue line), and Cu(111)/ZnO (red line). The reference zero of the energy scale corresponds to the energy of H_2O and CH_3OH in gas phase.

state (TS) and final state (FS) more than the initial state (IS) as compared to Cu(111) and CuZn(211). By examining the structures in Figures 3a and S1, we find that the H atom attaches to the O atom at the Cu/ZnO interface instead of Cu atoms on Cu(111) and CuZn(211) at the TSs and FSs. The clearly distinct structures significantly stabilize H at Cu/ZnO interface, as confirmed by the increased adsorption energy E_{ads}

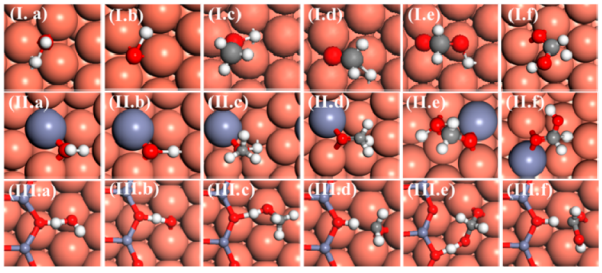

Figure 3. Structures at the transition states of (a) $H_2O^* + * \rightarrow OH^* + H^*$, (b) $OH^* + * \rightarrow O^* + H^*$, (c) $CH_3OH^* + * \rightarrow CH_3O^* + H^*$, (d) $CH_3O^* + * \rightarrow CH_2O^* + H^*$, (e) $H_2COOH^* + * \rightarrow H_2COO^* + H^*$, and (f) $H_2COOH^* + * \rightarrow HCOOH^* + H^*$ on Cu(111) (I), CuZn(211) (II), and Cu(111)/ZnO (III).

(by about 0.58 eV, Table 2) of H atom at the interfacial oxygen relative to Cu atoms on Cu(111) and CuZn(211). The

Table 2. Adsorption Energies (E_{ads} in eV) of the Possible Intermediates Involved in MSR on Cu(111), CuZn(211), and Cu(111)/ZnO at Their Most Favorable Sites

intermediates	Cu(111)	CuZn(211)	Cu(111)/ZnO
CH_3OH	−0.50	−0.73	−0.97
CH_3O	−2.78	−2.81	−3.02
CH_2O	−0.42	−0.60	−0.50
HCO	−1.59	−1.79	−1.69
H_2COOH	−2.67	−2.99	−3.13
H_2COO	−4.60	−5.08	−4.85
HCOOH	−0.50	−0.70	–
HCOO	−3.23	−3.54	−3.17
H_2O	−0.34	−0.52	−0.59
OH	−3.51	−3.68	−3.75
CO	−0.92	−0.90	−1.03
CO_2	−0.19	−0.21	−0.03
H	−0.18	−0.17	−0.75

differential charge density maps show considerable charge withdrawal (Bader charge) from H by interfacial O at Cu/ZnO interface (Figure 4a). However, charge builds up on H when

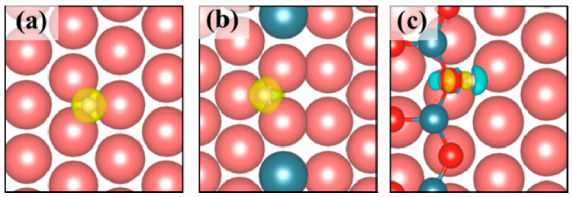

Figure 4. Differential charge density map for adsorption of H atom on (a) Cu(111) (with the isosufaces of 0.003 au), (b) CuZn(211) (with the isosufaces of 0.003 au), and (c) Cu(111)/ZnO (with the isosufaces of 0.01 au). Vermilion, blue, red, and white spheres represent Cu, Zn, O, and H, respectively. Blue and yellow insosurfaces indicate charge depletion and accumulation.

binding with Cu atoms on Cu(111) and CuZn(211) (Figures 4b and 4c), which reflects the different bond nature between H−O and H−Cu bond. In addition, unlike Cu and CuZn, which undergo the considerable rotation of the H−O axes for H−OH bond scission, there is little structural change at Cu/ZnO interface, contributing additionally to the substantial decrease in E_a (see Figure 3a). Likewise, the $OH^* + * \rightarrow O^* + H^*$ step is also largely enhanced on Cu/ZnO interface owing to the eletrophilicity of hydrogen, as shown in Figures 2a and 3b and Table 1. These findings are consistent with the favorable water dissociation observed on Cu/ZnO interface[19] and other interfaces between metal and metal oxides.[48,49]

For methanol dehydrogenation, it is found that the initial O−H bond breaking is more favorable than the initial C−H bond breaking regardless of the surface structure, consistent with the previous reports on Cu,[27] PdZn,[50,51] and ZnO supported single-atom catalysts.[52] Similarly to water, the O−H bond breaking in CH_3OH^* is also favorable at Cu/ZnO interface owing to the strong H−interfacial O bond and formation of favorable TS (Figures 2b and 3c). The barrier of 0.28 eV is significantly lower than that of 1.07 and 0.74 eV on Cu and CuZn, respectively. In contrast to the O−H bond scission, the C−H bond scission of CH_3O^* does not exhibit a strong

DOI: 10.1021/acs.jpcc.7b07703
J. Phys. Chem. C 2017, 121, 21553−21559

dependence on surface structure, with E_a differing by 0.06 eV at most on the three surfaces. Comparing the TS structures in Figures 3c and 3d, we find that the TS for the O−H bond scission of CH_3OH^* is reactant-like, while that for the $CH_3O^* + * \rightarrow CH_2O^* + H^*$ step is more product-like. The reason is that for O−H bond scission H prefers to bind with both O at the Cu/ZnO interface and in CH_3O^* intermediate at the TSs, which facilitates O−H bond scission. However, a favorable TS structure where H binds simultaneously with interfacial O (planar, graphite-like structure) and C (tetrahedral structure) in CH_2O^* is not available for C−H bond scission.

Once H_2O is activated and CH_2O is formed, the $OH^* + CH_2O^* \rightarrow H_2COOH^* + *$ step is quite facile on all the systems considered, with the barriers of no more than 0.38 eV. The facile recombinations of CH_2O^* and OH were also reported previously on Cu and ZnO supported single atoms for MSR.[27,52] Then, the resulting H_2COOH^* intermediate can proceed through either O−H bond scission forming H_2COO^* intermediate or C−H bond scission forming $HCOOH^*$ intermediate. As shown in Figure 5a and Table 1, Cu/ZnO

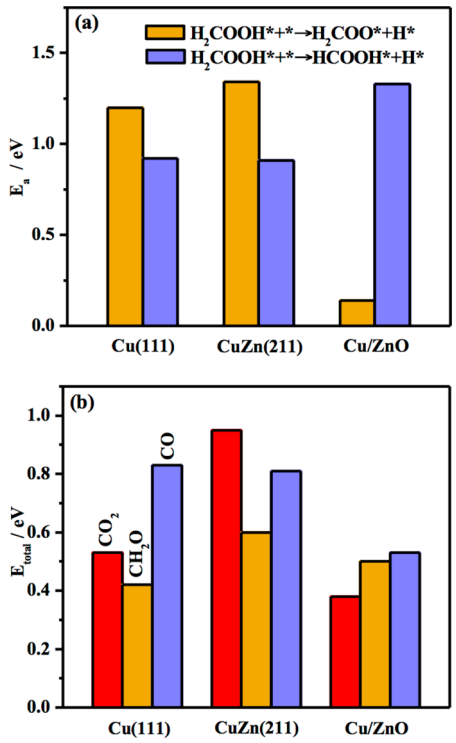

Figure 5. (a) Calculated barriers for C−H and O−H bond scission of H_2COOH^* intermediate. (b) Effective total barriers for CO_2, CH_2O, and CO formation with respect to $CH_2O^* + OH^*$.

interface prefers the former pathway, and the E_a of O−H bond scission is substantially lower than that of C−H bond scission by 1.19 eV. However, the latter pathway is more favorable on Cu and CuZn. The C−H bond scission of H_2COOH^* intermediate on the two surfaces has similar E_a of ∼0.90 eV, lower than the corresponding values of 1.20 and 1.34 eV for O−H bond scission.

The different dehydrogenation pathways between Cu/ZnO interface and Cu and CuZn alloy can be assigned to the high activity of interfacial O in the O−H bond scission (Figures 3e and 3f), as discussed above. Subsequently, the H_2COO^* intermediate on Cu/ZnO interface undergoes C−H bond scission (E_a = 0.91 eV), and $HCOOH^*$ intermediates on Cu and CuZn undergo O−H bond scission (E_a = 0.53 vs 0.62 eV), leading to $HCOO^*$ formation. The adsorbed $HCOO^*$ intermediate can decompose into H and CO_2, with the barriers of 1.26, 1.45, and 1.19 eV on Cu, CuZn, and Cu/ZnO interface, respectively. Finally, the H_2 desorption can be expected to be facile on these systems based on the calculated H_2 dissociative binding energies of −0.18 eV (Cu), −0.17 eV (CuZn), and −0.75 eV (Cu/ZnO interface) relative to 1/2 H_2 in gas phase. As the coverage of atomic H increases at the interface O (1/3−1 ML), H_2 dissociative binding energy decreases by 0.11 eV. Moreover, the entropic contribution of 0.73 eV per H_2 molecule at 500 K and standard pressure[53] can also provide additional driving force for H_2 desorption. In addition, the previous experimental and theoretical study on FeO(111) monolayer films on Pt(111) showed that the presence of O vacancy can enhance the H_2 formation and desorption.[54] Therefore, it can be expected that H_2 desorption could be further promoted by the presence of O vacancy on ZnO.

Besides OH* species, CH_2O^* can recombine with atomic O*, obtained either by the dissociation or by the disproportionation of OH*. The previous DFT study suggests that despite the relatively low barrier (0.25 eV) for OH disproportionation leads to H_2O formation,[27,31] which will be unfavorable as consideration of the reaction balance.[55] Thus, the O* species is not considered in this work.

The energy profiles for the most favorable CO_2 formation pathways on Cu(111), CuZn(211), and Cu/ZnO interface are illustrated in Figure 6. It is found that the stability of adsorbed

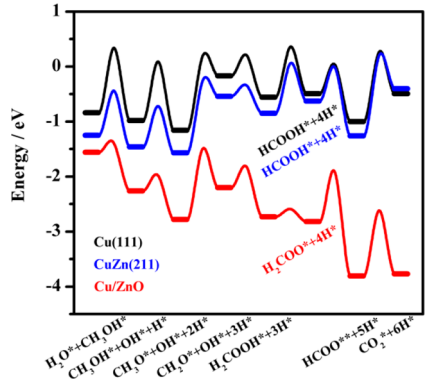

Figure 6. Energy profiles of methanol steam reforming on Cu(111) (black line), CuZn(211) (blue line), and Cu/ZnO (red line). The energy reference zero corresponds to the energy of H_2O and CH_3OH in gas phase.

intermediates generally follows the order of Cu(111) < CuZn(211) ≪ Cu/ZnO. Compared to Cu(111), CuZn(211) binds the intermediates modestly stronger (Table 2), which agrees well with previous DFT calculations by Studt et al.[15,39,56−58] Apart from Cu(111) and CuZn(211), they also consider Cu(211) and show that the bond strength of intermediates on Cu(211) is in between Cu(111) and CuZn(211). These results imply that both low coordination number of step and alloying with Zn contribute to the stronger intermediates binding on CuZn(211) than on Cu(111). On the Cu/ZnO interface, a significant enhancement of stability of intermediates, such as H*, CH_3OH^*, H_2COOH^*, and H_2O^*, is found. Compared to H*, which shows the largest increase in E_{ad} by 0.58 eV owing to strong H−interfacial O interaction,

DOI: 10.1021/acs.jpcc.7b07703
J. Phys. Chem. C 2017, 121, 21553−21559

CH_3OH, H_2COOH, and H_2O binding at the interface via H-bonding is less strengthened by 0.25−0.47 eV (Figure S1 and Table 2). These increased stabilities would ensure that the intermediates on Cu/ZnO interface would be found at higher surface coverages at equilibrium conditions. In addition, the barrier for O−H bond scission in H_2O*, CH_3OH*, and H_2COOH* is also greatly decreased on the interface, as discussed above, thereby accelerating the CO_2 formation. However, the barriers of the elementary steps on Cu and CuZn are comparable in magnitude, suggesting that the activity would not be affected significantly by alloying.

Having discussed the CO_2 formation, we now turn to its competitive pathways, namely formaldehyde and CO formation on Cu, CuZn, and Cu/ZnO interface. Note that formaldehyde (CH_2O*) is a key intermediate that is related to MSR selectivity. As shown above, it can recombine with OH*, followed by sequential H abstraction, leading to the formation of CO_2. In addition, the CH_2O* can also desorb or dehydrogenate, with the undesirable formation of CH_2O or CO. In the case of CO_2 formation, it is controlled by HCOOH* formation, HCOO* dehydrogenation, and CH_2O* recombination with OH* on Cu, CuZn, and Cu/ZnO interface, respectively (Figure 6). The calculated corresponding total barriers E_{total} on these systems are 0.53, 0.95, and 0.38 eV (Figure 5b), which are defined as the highest energies for CO_2 formation (HCOOH* formation, HCOO* dehydrogenation, and CH_2O* + OH*) relative to CH_2O* + OH*. The barrier of CH_2O* desorption is characterized by its adsorption energy, and the corresponding values are 0.42, 0.60, and 0.50 eV (Table 2). For CO formation, it is controlled by the CH_2O* + * → HCO* + H* step regardless of surface structures, and the total barriers with respect to CH_2O* are 0.83, 0.81, and 0.53 eV on Cu, CuZn, and Cu/ZnO interface, respectively. Two main features can be seen from Figure 5b: (1) CO formation is the least favorable on the three surfaces; (2) Cu and CuZn have higher selectivity toward CH_2O, whereas Cu/ZnO interface is more selective for CO_2 formation. The different selectivity of the three surfaces mainly originates from the significant enhancement of CO_2 formation by the electrophilicity of hydrogen at the interface.

Recently, Klotzer and co-workers[19] compared the MSR activity/selectivity of CuZn (≈10:1) surface alloy and pure Cu foil using temperature-programmed reaction in an UHV-compatible high-pressure cell operated as a recirculating batch reactor. They found that the initial CuZn (≈10:1) surface alloy provides an appropriate near-surface Zn loading for MSR-induced segregation to yield submonolayer Zn(Ox) coverage and therefore a high abundance of bimetallic-$Cu(Zn)^0$/Zn(Ox) interface at about 550 K. They proposed that the redox-active $Cu(Zn)^0$/Zn(Ox) sites assist in water activation and the transfer of hydroxide or oxygen to the latter, thus providing optimum conditions for higher CO_2 activity and selectivity. On clean Cu, dehydrogenation ceases with formaldehyde. These experimental findings are in excellent agreement with the present DFT calculations. Different from the experimental speculation of methanol dehydrogenation to formaldehyde on $Cu(Zn)^0$ regions, the present calculations show that it will take $Cu(Zn)^0$/Zn(Ox) sites as water activation. To provide a quantitative comparison with measurable kinetics, a kinetic Monte Carlo simulation would be crucial and be addressed in the future.

4. CONCLUSIONS

In summary, the distinct reactivities of the metallic copper, bimetallic copper−zinc alloy, and copper/zinc oxide interface coexisting under methanol steam reforming conditions are identified. Two different H species, namely those binding with O at Cu/ZnO interface and binding with metal on Cu and CuZn alloy, are differentiated and play an important role for overall activity and selectivity of MSR on zinc oxide supported copper catalysts. The strong interaction of H−interfacial O facilitates H adsorption and O−H bond scission in H_2O, CH_3OH, and H_2COOH, leading to the highest activity and selectivity toward CO_2 and H_2. In contrast, the weak H−metal interaction on Cu and CuZn alloy inhibits H adsorption and O−H bond scission, which results in the low activity and high selectivity toward CH_2O. Besides the reactivity, the different active sites for H binding also lead to variation in reaction pathway for CO_2 formation via H_2COO (Cu/ZnO interface) or HCOOH (Cu and CuZn alloy) intermediate. This work highlights the role of metal/oxide interface in improving reactivity of methanol steam reforming at the atomic level, and the insights achieved can be used for catalyst development in MSR and other energy conversion reactions of technological interest.

■ ASSOCIATED CONTENT

Supporting Information

The Supporting Information is available free of charge on the ACS Publications website at DOI: 10.1021/acs.jpcc.7b07703.

Configurations of the intermediates adsorption (Figure S1) and other transition states (Figure S2) involved in MSR on Cu(111), CuZn(211), and Cu/ZnO (PDF)

■ AUTHOR INFORMATION

Corresponding Author

*E-mail: wxli70@ustc.edu.cn.

ORCID

Hai-Yan Su: 0000-0001-9326-9647

Wei-Xue Li: 0000-0002-5043-3088

Author Contributions

The manuscript was written through contributions of all authors. All authors have given approval to the final version of the manuscript.

Author Contributions

⊥These authors contributed equally.

Notes

The authors declare no competing financial interest.

■ ACKNOWLEDGMENTS

We acknowledge funding from the Natural Science Foundation of China (91421315), the National Key R&D Program of China (2017YFB0602205, 2017YFA0204800), and the Chinese Academyof Sciences (QYZDJ-SSW-SLH054, XDA09030101).

■ REFERENCES

(1) Palo, D. R.; Dagle, R. A.; Holladay, J. D. Methanol Steam Reforming for Hydrogen Production. *Chem. Rev.* **2007**, *107*, 3992−4021.

(2) Yong, S. T.; Ooi, C. W.; Chai, S. P.; Wu, X. S. Review of Methanol Reforming-Cu-Based Catalysts, Surface Reaction Mechanisms, and Reaction Schemes. *Int. J. Hydrogen Energy* **2013**, *38*, 9541−9552.

DOI: 10.1021/acs.jpcc.7b07703
J. Phys. Chem. C 2017, 121, 21553−21559

(3) Sa, S.; Silva, H.; Brandao, L.; Sousa, J. M.; Mendes, A. Catalysts for Methanol Steam Reforming-a Review. *Appl. Catal., B* **2010**, *99*, 43−57.
(4) Lemons, R. A. Fuel Cells for Transportation. *J. Power Sources* **1990**, *29*, 251−264.
(5) Acres, G. J. K.; Frost, J. C.; Hards, G. A.; Potter, R. J.; Ralph, T. R.; Thompsett, D.; Burstein, G. T.; Hutchings, G. J. Electrocatalysts for Fuel Cells. *Catal. Today* **1997**, *38*, 393−400.
(6) Alayoglu, S.; Nilekar, A. U.; Mavrikakis, M.; Eichhorn, B. Ru-Pt Core-Shell Nanoparticles for Preferential Oxidation of Carbon Monoxide in Hydrogen. *Nat. Mater.* **2008**, *7*, 333−338.
(7) Peppley, B. A.; Amphlett, J. C.; Kearns, L. M.; Mann, R. F. Methanol-Steam Reforming on Cu/ZnO/Al2O3. Part 1: The Reaction Network. *Appl. Catal., A* **1999**, *179*, 21−29.
(8) Peppley, B. A.; Amphlett, J. C.; Kearns, L. M.; Mann, R. F. Methanol-Steam Reforming on Cu/ZnO/Al2O3 Catalysts. Part 2. A Comprehensive Kinetic Model. *Appl. Catal., A* **1999**, *179*, 31−49.
(9) Grunwaldt, J. D.; Molenbroek, A. M.; Topsøe, N. Y.; Topsøe, H.; Clausen, B. S. In Situ Investigations of Structural Changes in Cu/ZnO Catalysts. *J. Catal.* **2000**, *194*, 452−460.
(10) Günter, M. M.; Ressler, T.; Jentoft, R. E.; Bems, B. Redox Behavior of Copper Oxide/Zinc Oxide Catalysts in the Steam Reforming of Methanol Studied by in Situ X-Ray Diffraction and Absorption Spectroscopy. *J. Catal.* **2001**, *203*, 133−149.
(11) Agrell, J.; Birgersson, H.; Boutonnet, M. Steam Reforming of Methanol over a Cu/ZnO/Al2O3 Catalyst: A Kinetic Analysis and Strategies for Suppression of CO Formation. *J. Power Sources* **2002**, *106*, 249−257.
(12) Hansen, P. L.; Wagner, J. B.; Helveg, S.; Rostrup-Nielsen, J. R.; Clausen, B. S.; Topsøe, H. Atom-Resolved Imaging of Dynamic Shape Changes in Supported Copper Nanocrystals. *Science* **2002**, *295*, 2053−2055.
(13) Grabow, L. C.; Mavrikakis, M. Mechanism of Methanol Synthesis on Cu through CO2 and CO Hydrogenation. *ACS Catal.* **2011**, *1*, 365−384.
(14) Zhao, Y.-F.; Yang, Y.; Mims, C.; Peden, C. H. F.; Li, J.; Mei, D. Insight into Methanol Synthesis from CO2 Hydrogenation on Cu(111): Complex Reaction Network and the Effects of H2O. *J. Catal.* **2011**, *281*, 199−211.
(15) Behrens, M.; Studt, F.; Kasatkin, I.; Kuehl, S.; Haevecker, M.; Abild-Pedersen, F.; Zander, S.; Girgsdies, F.; Kurr, P.; Kniep, B.-L. The Active Site of Methanol Synthesis over Cu/ZnO/Al2O3 Industrial Catalysts. *Science* **2012**, *336*, 893−897.
(16) Kuld, S.; Thorhauge, M.; Falsig, H.; Elkjaer, C. F.; Helveg, S.; Chorkendorff, I.; Sehested, J. Quantifying the Promotion of Cu Catalysts by ZnO for Methanol Synthesis. *Science* **2016**, *352*, 969−974.
(17) van den Berg, R.; Prieto, G.; Korpershoek, G.; van der Wal, L. I.; van Bunningen, A. J.; Laegsgaard-Jorgensen, S.; de Jongh, P. E.; de Jong, K. P. Structure Sensitivity of Cu and CuZn Catalysts Relevant to Industrial Methanol Synthesis. *Nat. Commun.* **2016**, *7*, 13057.
(18) Kattel, S.; Ramirez, P. J.; Chen, J. G.; Rodriguez, J. A.; Liu, P. Catalysis Active Sites for CO2 Hydrogenation to Methanol on Cu/ZnO Catalysts. *Science* **2017**, *355*, 1296−1299.
(19) Rameshan, C.; Stadlmayr, W.; Penner, S.; Lorenz, H.; Memmel, N.; Havecker, M.; Blume, R.; Teschner, D.; Rocha, T.; Zemlyanov, D. Hydrogen Production by Methanol Steam Reforming on Copper Boosted by Zinc-Assisted Water Activation. *Angew. Chem., Int. Ed.* **2012**, *51*, 3002−3006.
(20) Chen, Z. X.; Lim, K. H.; Neyman, K. M.; Rosch, N. Effect of Steps on the Decomposition of CH3O at PdZn Alloy Surfaces. *J. Phys. Chem. B* **2005**, *109*, 4568−4574.
(21) Xu, L.; Mei, D.; Henkelman, G. Adaptive Kinetic Monte Carlo Simulation of Methanol Decomposition on Cu(100). *J. Chem. Phys.* **2009**, *131*, 244520.
(22) Mei, D.; Xu, L.; Henkelman, G. Potential Energy Surface of Methanol Decomposition on Cu(110). *J. Phys. Chem. C* **2009**, *113*, 4522−4537.
(23) Zuo, Z.-J.; Wang, L.; Han, P.-D.; Huang, W. Insights into the Reaction Mechanisms of Methanol Decomposition, Methanol Oxidation and Steam Reforming of Methanol on Cu(111): A Density Functional Theory Study. *Int. J. Hydrogen Energy* **2014**, *39*, 1664−1679.
(24) Gokhale, A. A.; Dumesic, J. A.; Mavrikakis, M. On the Mechanism of Low-Temperature Water Gas Shift Reaction on Copper. *J. Am. Chem. Soc.* **2008**, *130*, 1402−1414.
(25) Papavasiliou, J.; Avgouropoulos, G.; Ioannides, T. Steady-State Isotopic Transient Kinetic Analysis of Steam Reforming of Methanol over Cu-Based Catalysts. *Appl. Catal., B* **2009**, *88*, 490−496.
(26) Gu, X.-K.; Li, W.-X. First-Principles Study on the Origin of the Different Selectivities for Methanol Steam Reforming on Cu(111) and Pd(111). *J. Phys. Chem. C* **2010**, *114*, 21539−21547.
(27) Lin, S.; Johnson, R. S.; Smith, G. K.; Xie, D.; Guo, H. Pathways for Methanol Steam Reforming Involving Adsorbed Formaldehyde and Hydroxyl Intermediates on Cu(111): Density Functional Theory Studies. *Phys. Chem. Chem. Phys.* **2011**, *13*, 9622−9631.
(28) Lin, S.; Xie, D.; Guo, H. Methyl Formate Pathway in Methanol Steam Reforming on Copper: Density Functional Calculations. *ACS Catal.* **2011**, *1*, 1263−1271.
(29) Kuld, S.; Conradsen, C.; Moses, P. G.; Chorkendorff, I.; Sehested, J. Quantification of Zinc Atoms in a Surface Alloy on Copper in an Industrial-Type Methanol Synthesis Catalyst. *Angew. Chem., Int. Ed.* **2014**, *53*, 5941−5945.
(30) Lunkenbein, T.; Schumann, J.; Behrens, M.; Schloegl, R.; Willinger, M. G. Formation of a ZnO Overlayer in Industrial Cu/Zno/Al2O3 Catalysts Induced by Strong Metal-Support Interactions. *Angew. Chem., Int. Ed.* **2015**, *54*, 4544−4548.
(31) Tang, Q.-L.; Chen, Z.-X. Influence of Aggregation, Defects, and Contaminant Oxygen on Water Dissociation at Cu(110) Surface: A Theoretical Study. *J. Chem. Phys.* **2007**, *127*, 104707−104716.
(32) Deng, X.; Yao, K.; Sun, K.; Li, W.-X.; Lee, J.; Matranga, C. Growth of Single- and Bilayer Zno on Au(111) and Interaction with Copper. *J. Phys. Chem. C* **2013**, *117*, 11211−11218.
(33) Schott, V.; Oberhofer, H.; Birkner, A.; Xu, M.; Wang, Y.; Muhler, M.; Reuter, K.; Woell, C. Chemical Activity of Thin Oxide Layers: Strong Interactions with the Support Yield a New Thin-Film Phase of Zno. *Angew. Chem., Int. Ed.* **2013**, *52*, 11925−11929.
(34) Halevi, B.; Lin, S.; Roy, A.; Zhang, H.; Jeroro, E.; Vohs, J.; Wang, Y.; Guo, H.; Datye, A. K. High Co2selectivity of Zno Powder Catalysts for Methanol Steam Reforming. *J. Phys. Chem. C* **2013**, *117*, 6493−6503.
(35) Kresse, G.; Furthmuller, J. Efficiency of Ab-Initio Total Energy Calculations for Metals and Semiconductors Using a Plane-Wave Basis Set. *Comput. Mater. Sci.* **1996**, *6*, 15−50.
(36) Klimes, J.; Bowler, D. R.; Michaelides, A. Van Der Waals Density Functionals Applied to Solids. *Phys. Rev. B: Condens. Matter Mater. Phys.* **2011**, *83*, 195131−195143.
(37) Blochl, P. E. Projector Augmented-Wave Method. *Phys. Rev. B: Condens. Matter Mater. Phys.* **1994**, *50*, 17953−17979.
(38) Perdew, J. P.; Burke, K.; Ernzerhof, M. Generalized Gradient Approximation Made Simple. *Phys. Rev. Lett.* **1996**, *77*, 3865−3868.
(39) Studt, F.; Abild-Pedersen, F.; Varley, J. B.; Nørskov, J. K. CO and CO2 Hydrogenation to Methanol Calculated Using the Beef-Vdw Functional. *Catal. Lett.* **2013**, *143*, 71−73.
(40) Tusche, C.; Meyerheim, H. L.; Kirschner, J. Observation of Depolarized Zno(0001) Monolayers: Formation of Unreconstructed Planar Sheets. *Phys. Rev. Lett.* **2007**, *99*, 026102−026105.
(41) Weirum, G.; Barcaro, G.; Fortunelli, A.; Weber, F.; Schennach, R.; Surnev, S.; Netzer, F. P. Growth and Surface Structure of Zinc Oxide Layers on a Pd(111) Surface. *J. Phys. Chem. C* **2010**, *114*, 15432−15439.
(42) Monkhorst, H. J.; Pack, J. D. Special Points for Brillouin-Zone Integrations. *Phys. Rev. B* **1976**, *13*, 5188−5192.
(43) Sun, K. J.; Zhao, Y. H.; Su, H.-Y.; Li, W.-X. Force Reversed Method for Locating Transition States. *Theor. Chem. Acc.* **2012**, *131*, 1118−1127.
(44) Henkelman, G.; Jonsson, H. Improved Tangent Estimate in the Nudged Elastic Band Method for Finding Minimum Energy Paths and Saddle Points. *J. Chem. Phys.* **2000**, *113*, 9978−9985.

DOI: 10.1021/acs.jpcc.7b07703
J. Phys. Chem. C 2017, 121, 21553−21559

(45) Henkelman, G.; Uberuaga, B. P.; Jonsson, H. A Climbing Image Nudged Elastic Band Method for Finding Saddle Points and Minimum Energy Paths. *J. Chem. Phys.* **2000**, *113*, 9901−9904.
(46) Janotti, A.; Van de Walle, C. G. Native Point Defects in ZnO. *Phys. Rev. B: Condens. Matter Mater. Phys.* **2007**, *76*, 165202−165223.
(47) Barcaro, G.; Thomas, I. O.; Fortunelli, A. Validation of Density-Functional Versus Density-Functional+ U Approaches for Oxide Ultrathin Films. *J. Chem. Phys.* **2010**, *132*, 124703.
(48) Gu, X. K.; Ouyang, R.; Sun, D.; Su, H. Y.; Li, W. X. Co Oxidation at the Perimeters of an FeO/Pt (111) Interface and How Water Promotes the Activity: A First-Principles Study. *ChemSusChem* **2012**, *5*, 871−878.
(49) Rodriguez, J. A.; Liu, P.; Hrbek, J.; Evans, J.; Perez, M. Water Gas Shift Reaction on Cu and Au Nanoparticles Supported on CeO2 (111) and ZnO (0001): Intrinsic Activity and Importance of Support Interactions. *Angew. Chem., Int. Ed.* **2007**, *46*, 1329−1332.
(50) Huang, Y.; He, X.; Chen, Z.-X. Density Functional Study of Methanol Decomposition on Clean and O or OH Adsorbed Pdzn(111). *J. Chem. Phys.* **2013**, *138*, 184701−184707.
(51) Smith, G. K.; Lin, S.; Lai, W.; Datye, A.; Xie, D.; Guo, H. Initial Steps in Methanol Steam Reforming on Pdzn and Zno Surfaces: Density Functional Theory Studies. *Surf. Sci.* **2011**, *605*, 750−759.
(52) Gu, X. K.; Qiao, B. T.; Huang, C. Q.; Ding, W. C.; Sun, K. J.; Zhan, E. S.; Zhang, T.; Liu, J. Y.; Li, W. X. Supported Single Pt-1/Au-1 Atoms for Methanol Steam Reforming. *ACS Catal.* **2014**, *4*, 3886−3890.
(53) Gu, X. K.; Liu, B.; Greeley, J. First-Principles Study of Structure Sensitivity of Ethylene Glycol Conversion on Platinum. *ACS Catal.* **2015**, *5*, 2623−2631.
(54) Xu, L. S.; Zhang, W. H.; Zhang, Y. L.; Wu, Z. F.; Chen, B. H.; Jiang, Z. Q.; Ma, Y. S.; Yang, J. L.; Huang, W. X. Oxygen Vacancy-Controlled Reactivity of Hydroxyls on an FeO(111) Monolayer Film. *J. Phys. Chem. C* **2011**, *115*, 6815−6824.
(55) Lim, K. H.; Moskaleva, L. V.; Rosch, N. Surface Composition of Materials Used as Catalysts for Methanol Steam Reforming: A Theoretical Study. *ChemPhysChem* **2006**, *7*, 1802−1812.
(56) Studt, F.; Abild-Pedersen, F.; Wu, Q.; Jensen, A. D.; Temel, B.; Grunwaldt, J.-D.; Nørskov, J. K. CO Hydrogenation to Methanol on Cu−Ni Catalysts: Theory and Experiment. *J. Catal.* **2012**, *293*, 51−60.
(57) Kunkes, E. L.; Studt, F.; Abild-Pedersen, F.; Schlögl, R.; Behrens, M. Hydrogenation of CO2 to Methanol and CO on Cu/ZnO/Al2O3: Is There a Common Intermediate or Not? *J. Catal.* **2015**, *328*, 43−48.
(58) Studt, F.; Behrens, M.; Kunkes, E. L.; Thomas, N.; Zander, S.; Tarasov, A.; Schumann, J.; Frei, E.; Varley, J. B.; Abild-Pedersen, F. The Mechanism of CO and CO2 Hydrogenation to Methanol over Cu-Based Catalysts. *ChemCatChem* **2015**, *7*, 1105−1111.

DOI: 10.1021/acs.jpcc.7b07703
J. Phys. Chem. C 2017, 121, 21553−21559